Journal of the Serbian Chemical Society
JSCS@tmf.bg.ac.rs • www.shd.org.rs/JSCS
J. Serb. Chem. Soc. *87* (5) S104–S116 (2022) *Supplementary material*

SUPPLEMENTARY MATERIAL TO

Structural, biological and computational study of oxamide derivative

IGNJAT P. FILIPOVIĆ[1], EMINA M. MRKALIĆ[2], GIORGIO PELOSI[3], VESNA KOJIĆ[4], DIMITAR JAKIMOV[4], DEJAN BASKIĆ[5] and ZORAN D. MATOVIĆ[1]*

[1]*University of Kragujevac, Faculty of Science, Department of Chemistry, Radoja Domanovića 12, 34000 Kragujevac, Serbia,* [2]*University of Kragujevac, Institute for Information Technologies, Department of Science, Jovana Cvijića bb, Kragujevac 34000, Serbia,* [3]*Department of Chemistry, Life Sciences and Environmental Sustainability, University of Parma, 43123 Parma, Italy,* [4]*Institute of Oncology Sremska Kamenica, Novi Sad, Institutski put 4, 21204 Sremska Kamenica, Serbia and* [5]*University of Kragujevac, Faculty of Medicinal Science, S. Markovića 69, 34000 Kragujevac, Serbia*

J. Serb. Chem. Soc. *87* (5) (2022) 545–559

Docking

The protein target was prepared from the file in PDB format downloaded directly from the RSCB PDB site (PDB entry 3LDL) using AutoDock Tools. Because 3LDL is dimer, monomers were separated and only the A chain was used in further preparation. The co-crystalized ligand and water molecules were removed. Hydrogen atoms were added, Gasteiger charges were calculated, non-polar hydrogen atoms were merged and AD4 atom types were assigned to all atoms. The co-crystalized ATP molecule was used to validate the docking method after B3LYP/TZVP QM calculations from which partial charges for its atoms were obtained. Partial charges for atoms in H_2obbz^{2-} and H_4obbz structures were obtained using the same method. Non-polar hydrogens were merged, and all torsional rotations were enabled except for torsions in the amide bonds (H-N-C-O) as per default preparation options. Averaged coordinates of co-crystalized ATP were used as the center for the grid box.

Lamarckian algorithm (genetic algorithm (GA) - local search (LS) hybrid) was used for all experiments with AutoDock4. To increase the chance of finding the best solution, the number of GA-LS runs in each experiment was set to 20, the number of individuals in each generation was set to 300, the maximum number of energy evaluations per run was set to 25 million, and all other settings were set to default. Docking with Vina was done with most of the parameters at

* Corresponding author. E-mail: zmatovic@kg.ac.rs

default values, except exhaustiveness that was set to 16 to increase precision. Both Vina and AD4 managed to replicate the mode of binding between Grp-78 and ATP found in the crystal structure. This is shown in Fig. S-1.

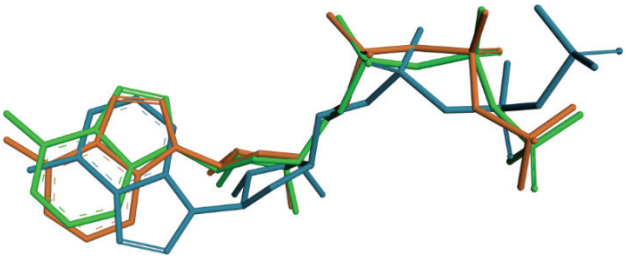

Fig. S-1. Comparison of ATP structure derived from crystal with structures from best docking solutions. Green - crystal; Orange - Vina; Blue - AD4.

Molecular dynamics

Ligand Gaussian09 Rev E.01[1] was used for the QM calculation for parameterization. AmberTools21[2] was used for the structural modeling and data analyses while pmemd.cuda[3,4] in AMBER20[2] was employed in the MD simulation. The three ligands were modeled as described below. The structure of each ligand was optimized based on the B3LYP[5-7]/TZVP[8] level of theory. Antechamber[9] in AmberTools21 was used for performing the RESP charge fitting for the three ligands. The bond, angle and torsion parameters about the ligands were based on general amber force field (GAFF,[10] version 1.8) while the protein system was modeled by the ff19SB force field. To test the quality of the developed force field for the ligands, RMSD calculation was performed between the QM optimized and MM minimized structures. The MM minimization was performedmby using the nucleic acid builder (NAB) module in AmberTools21: the first minimization was performed employing the conjugated minimization algorithm with a convergence criteria of energy gradient as $2.1 \cdot 10^{-4}$ kJ mol^{-1} Å^{-1} and maximum 20000 steps, afterwards another minimization was performed using the Newton-Raphson algorithm with treating the convergence criteria of energy gradient as $8.3 \cdot 10^{-12}$ kJ mol^{-1} Å^{-1} and a maximum of 50 steps. The *RMSD* values of MM minimized structures of ATP, H_2obbz^{2-} and H_4obbz ligands are 0.53, 0.56 and 0.23 Å, respectively, when comparing to the QM optimized ones. To further validate the parameterization, normal mode analyses were performed based on the MM level and compared to the QM calculated results. The R^2 values of the linear fittings between MM and QM calculated normal mode frequencies (aligned based on the frequency values) about ATP, H_2obbz^{2-} and H_4obbz compounds are 0.9961, 0.9815 and 0.9873, respectively. The *RMSD* values for different ligands are given in Fig. S-2. Based on these

parameterizations, modeling, minimization, MD simulations and MMPBSA/ /MMGBSA analyses were started.

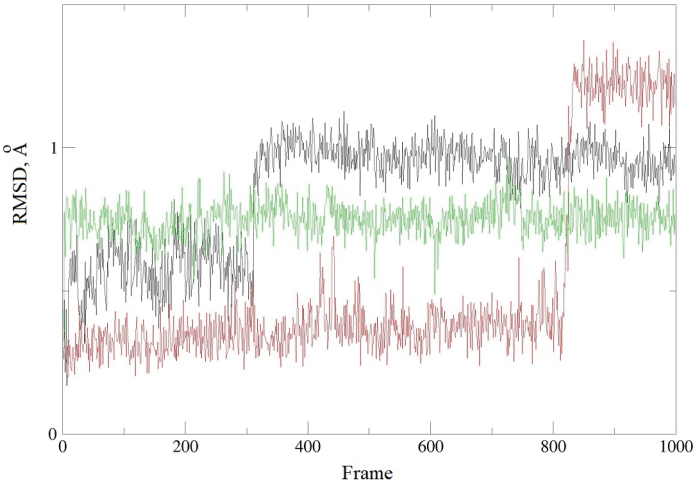

Fig. S-2. *RMSD* values of minimized solvated ligands.

Protein. The original structures of the protein-ligand complexes were prepared using the best hit from AutoDock4[11] run performed on selected target (PDB code 3LDL[12]). Afterwards these structures were adjusted based on the amino acid library in AMBER force field. A rectangular TIP4 OPC[13] water box (~75×72×50 Å) was used to solvate the system with all the water molecules are at least 1.5 Å away from the protein. Then Na+ ions were added to neutralize the negative charged system (3LD-ATP (-6), 3LDL-H_2obbz (-4) and 3LDL-H_4obbz (-2)) with their van der Waals parameters were from Li *et al.*[14] Afterwards 4 stages of minimization were carried out to optimize geometry of the solvated protein-ligand complex system. 1000 steps of steepest descend minimization plus 1000 steps of conjugated minimization were performed for each of the first three stages. 47.8 mol J^{-1} $Å^{-2}$ restraints were added to the all the atoms in the protein-ligand complex in the first stage, heavy atoms in the protein-ligand complex in the second stage while backbone C, CA and N atoms in the protein and non-metallic heavy atoms in the ligand for the third stage, respectively. The fourth stage of minimization was performed by 2000 steps of steepest descend minimization and afterwards 3000 steps of conjugated minimization with 4.78 mol kJ^{-1} $Å^{-2}$ restraints on the backbone N, CA and C atoms as well as non-metallic heavy atoms in the ligand. After that 1 ns MD simulation was performed in NVT ensemble to heat the system from 0 to 303.15 K followed by 1 ns MD simulation of equilibration carried out at 303.15 K in NVT ensemble. Afterwards 1 ns MD simulation was performed under 303.15 K and 1 atmosphere in NPT

ensemble to correct the density and further equilibrate the system. All above MD simulations were performed with 42 mol kJ^{-1} Å^{-2} restraints on the backbone N, CA and C atoms as well as the non-metallic heavy atoms in the ligand, referencing from the initial structure of each running. In the end 20 ns MD simulation of sampling was performed under 303.15 K in NPT ensemble without any restraints. Snapshots were saved for each 20 ps with totally 1000 snapshots were collected for the further analysis. Former research showed that multiple independent samplings could offer better results.[17] Here we ran 5 independent runs for each complex, totally there are 10000 snapshots along 100 ns sampling was collected for each complex. Particle mesh Ewald (PME) approach,[15-17] periodic boundary condition and 12 Å cut off were used during all the simulation. SHAKE[18] was used to constrain the bond lengths of heavy atoms and hydrogen atoms with a tolerance as 10^{-5} Å, while a three-point algorithm was used for water molecules.[19] Temperature was controlled by Langevin algorithm with collision frequency as 1.0 ps^{-1} in all the MD simulations. Pressure was controlled by using Berendsen barostat[20] with pressure relaxation time as 1.0 ps in the NPT production step.

To calculate the binding free energies between 3LDL monomer and each ligand, MMGBSA and MMPBSA analyses were carried out by using MMPBSA.py[21] in AmberTools21. GB model from Hawkins *et al.*[22,23] was used for the MMGBSA analyses by using the parameters from Tsui and Case[24] with treating salt concentration as 0.15 M. MMPBSA analyses were performed with 0.15 M ionic strength, 0.021 kJ mol^{-1}·Å^{-2} surface tension and without correction of free energy contribution from non-polar interaction. Normal mode analyses (NMA) were performed with 0.1 M ionic strength at 298.15 K by using the same GB model used in the MMGBSA analyses.

TABLE S-I. Δ*G* binding energies obtained by MMGBSA method (Energy differences are averaged over simulation run)

Energy components[a]	Average energy, kJ mol^{-1}		
	ATP	H_2obbz^{2-}	H_4obbz
VDWAALS	-207.93	-153.99	-191.51
EEL	-445.48	-320.76	-206.54
EGB	619.41	392.97	283.37
ESURF	-27.12	-22.24	-25.32
Δ*G* gas	-653.42	-474.75	-398.06
Δ*G* solv	592.29	370.73	258.06
Δ*G* binding	**-61.12**	**-104.02**	**-140.00**

[a]*VDWAALS* - van der Waals energy; *EEL* - electrostatic energy; *EGB* - polar solvation energy; *ESURF* - solvent-accessible surface area term; Δ*G* gas - Total free energy in gas phase; Δ*G* solv - Total free energy in solvent; Δ*G* binding - Estimated binding free energy calculated form the terms above.

Crucial interactions with amino-acid residues from frames with the lowest binding energy are shown in Fig. S-3.

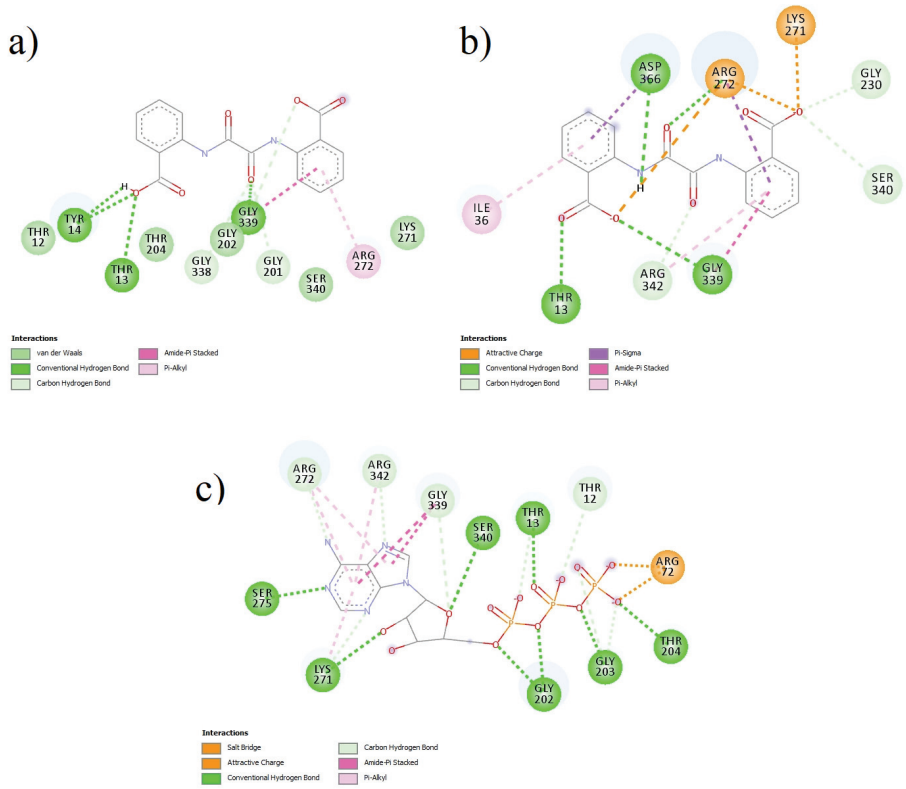

Fig. S-3. Crucial interactions of ligands with Grp78 during MD simulations. a) H_4obbz; b) H_2obbz^{2-}; c) ATP.

Biology

Cell lines: The cell lines used in the study were MCF-7 (human breast adenocarcinoma), A549 (human lung carcinoma), HT-29 (human colon adenocarcinoma), HeLa (human cervix adenocarcinoma) and MRC-5 (human foetal lung fibroblasts). The cells were grown in Dulbecco's modified Eagle's medium (DMEM) with 4.5 % of glucose, supplemented with 10 % of fetal bovine serum (FBS, Sigma) and antibiotics and antimicotics solution (Sigma). All cell lines were cultivated at 37 °C in an atmosphere of 5 % CO_2 and absolute humidity.

MTT assay: Growth inhibition was evaluated by tetrazolium colorimetric MTT assay (SIGMA). Exponentially growing cells were harvested and plated into 96-well microtiter plates (Costar) at optimal seeding density of 10^4 cells per well. Tested substances, at tenfold the required final concentration, were added

(10 µl/well) to all wells except to the control ones and microplates were incubated for 48 h. Three hours before the end of incubation period, 10 µl of MTT (5mg/ml) solution was added to all wells. Acid-isopropanol (100 µl of 0.04 M HCl in isopropanol) was added to all wells and mixed thoroughly to dissolve the dark blue crystals. After a few minutes at room temperature, to ensure that all crystals were dissolved, the plates were read on a spectrophotometer plate reader (Multiscan MCC340, Labsystems) at 540/690 nm. The inhibition of growth was expressed as a percent of a control and cytotoxicity was calculated according to the formula: $((1 - A_{test})/A_{control})100$. Two independent experiments were set out with quadruplicate wells for each concentration of the compound. The IC_{50} of compounds was determined by Median effect analysis.[25]

Annexin V-FITC/7-AAD assay for determination of apoptosis and necrosis by flow cytometry: Staining was performed according to manufacturer's protocol (Beckman Coulter, USA). Briefly, HeLa cells were treated with **(1)** in concentration equivalent to IC50 value, or media alone (control). After treatment (48 h, 37 ºC, 5 % CO_2, absolute humidity) cells were collected, washed in PBS and finally cell pellet was resuspended in ice cold binding buffer. Cell suspension ($1 \cdot 10^5$ cells) was stained with Annexin V-FITC and 7-AAD following the manufacturer's instruction. Samples were evaluated using flow cytometer (Cytomics FC500, Beckman Coulter, USA). The percentage of viable cells (AnnV-/7AAD-), early apoptotic (AnnV+/7AAD-), late apoptotic (AnnV+/7-AAD+) and necrotic cells (AnnV-/7-AAD+) was determined by Flowing Software (http://www.flowingsoftware.com/) and results were presented as dot plots.

Western blot analysis: Cells were seeded in 6-well plates at a concentration of $5 \cdot 10^5$ cells/well and treated with doxorubicin and tested compounds or media alone (control) for 48 h. The protein concentration in cell lysate was determined by Bradford protein assay in a 96-well microtiter plate (ThermoLab Systems, Multiscan Accent spectrophotometer) using bovine serum albumin as the standard. Molecular mass markers for proteins were obtained from Amersham Biosciences. For the Western blot, 50 µg of proteins per sample were separated by electrophoresis and electro-transferred to a polyvinylidene difluoride (PVDF) membrane Hybond-P (Amersham Biosciences, Arlington Heights, IL) and then blotted with primary antibodies (Bcl-2, PARP, Caspase-3, and Actin). Monoclonal antibodies against human Bcl-2 and Caspase 3 were obtained from R&D Systems (Minneapolis, MN). Anti- poly (ADP-ribose) polymerase (PARP) was purchased from Santa Cruz Biotechnology (Santa Cruz, CA). Antibody against α-actin, β-actin or γ-actin was purchased from Sigma Chemical (St. Louis, MO). Proteins were detected by an enhanced chemiluminescence (ECL Plus) kit (Amersham Biosciences), that includes peroxidase-labeled donkey anti-

rabbit and sheep anti-mouse secondary antibodies. Blots were developed with an ECL Plus detection system and recorded on Hyperfilm (Amersham Biosciences).

Cell cycle Analysis by flow cytometry: Cell cycle analysis was performed as described previously.[26] HeLa cells were incubated with media alone (control) or with **(1)** in concentration corresponding to IC50 value, for 48 h at 37 °C in 5 % CO_2. Treated cells were harvested, washed in PBS and finally fixed overnight in ice cold 70 % ethanol. After fixation, cells were washed, resuspended in PBS containing 500 μg mL^{-1} RNAseA and incubated 30 minutes at 37 °C in the dark. Staining was performed with 5 μL of propidium iodide (10mg/mL). After 15 minutes of incubation in the dark, cells were immediately analyzed by Cytomics FC500 flow cytometer (Beckman Coulter, USA). DNA content was defined by Flowing Software (http://www.flowingsoftware.com/) and cell cycle distribution was illustrated as histograms.

Infrared spectra

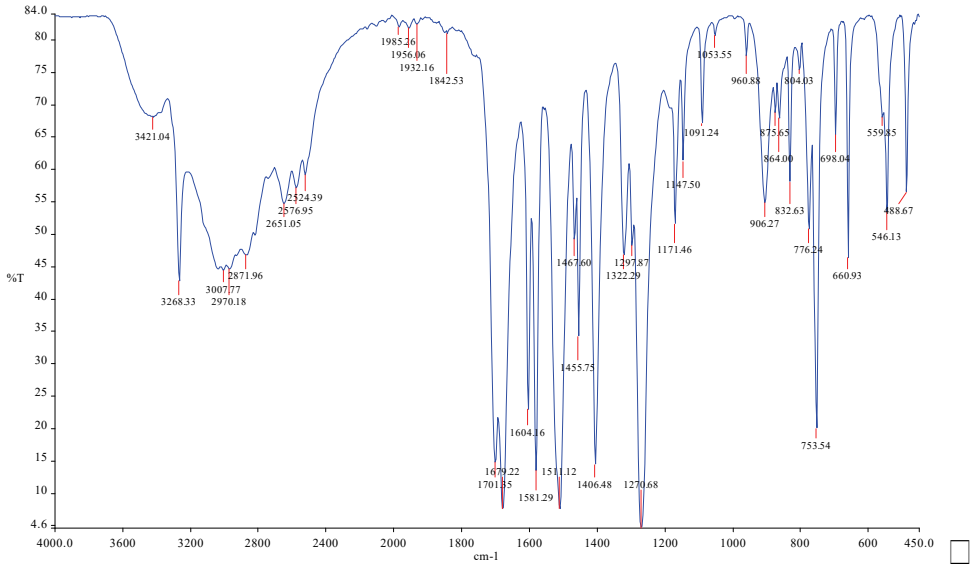

Fig. S-4. IR spectrum of H_4obbz ligand.

Crystal structure

TABLE S-II. Bond lengths in compound **(2)**

Atom 1	Atom 2	Type	Length, Å
C1	C2	Single	1.49(1)
C1	O1	Delocalised	1.249(8)
C1	O2	Delocalised	1.258(9)
C2	C3	Aromatic	1.421(7)
C2	C7	Aromatic	1.382(8)
C3	C4	Aromatic	1.37(1)
C3	N1	Single	1.410(7)
C4	H6	Single	0.930
C4	C5	Aromatic	1.39(1)
C5	H7	Single	0.930
C5	C6	Aromatic	1.384(9)
C6	H1A	Single	0.931
C6	C7	Aromatic	1.38(1)
C7	H5	Single	0.930
C8	N1	Single	1.332(7)
C8	O3	Double	1.23(1)
C8	C8	Single	1.53(1)
N1	H1	Single	0.861
C1	C2	Single	1.49(1)
C1	O1	Delocalised	1.249(8)
C1	O2	Delocalised	1.258(9)
C2	C3	Aromatic	1.421(7)
C2	C7	Aromatic	1.382(8)
C3	C4	Aromatic	1.37(1)
C3	N1	Single	1.410(7)
C4	H6	Single	0.930
C4	C5	Aromatic	1.39(1)
C5	H7	Single	0.930
C5	C6	Aromatic	1.384(9)
C6	H1A	Single	0.931
C6	C7	Aromatic	1.38(1)
C7	H5	Single	0.930
C8	N1	Single	1.332(7)
C8	O3	Double	1.23(1)
N1	H1	Single	0.861

TABLE S-III. Angles in compound **(2)**

Atom 1	Atom 2	Atom 3	Angle, °
C2	C1	O1	118.2(6)
C2	C1	O2	119.9(6)
O1	C1	O2	121.9(7)
C1	C2	C3	124.5(5)
C1	C2	C7	117.3(5)
C3	C2	C7	118.2(5)
C2	C3	C4	120.1(5)

Atom 1	Atom 2	Atom 3	Angle, °
C2	C3	N1	117.7(5)
C4	C3	N1	122.2(5)
C3	C4	H6	119.8
C3	C4	C5	120.2(6)
H6	C4	C5	120.0
C4	C5	H7	119.7
C4	C5	C6	120.6(7)
H7	C5	C6	119.7
C5	C6	H1A	120.5
C5	C6	C7	118.9(7)
H1A	C6	C7	120.5
C2	C7	C6	122.0(6)
C2	C7	H5	118.9
C6	C7	H5	119.1
N1	C8	O3	127.4(6)
N1	C8	C8	111.5(5)
O3	C8	C8	121.0(6)
C3	N1	C8	129.8(5)
C3	N1	H1	115.1
C8	N1	H1	115.2
C2	C1	O1	118.2(6)
C2	C1	O2	119.9(6)
O1	C1	O2	121.9(7)
C1	C2	C3	124.5(5)
C1	C2	C7	117.3(5)
C3	C2	C7	118.2(5)
C2	C3	C4	120.1(5)
C2	C3	N1	117.7(5)
C4	C3	N1	122.2(5)
C3	C4	H6	119.8
C3	C4	C5	120.2(6)
H6	C4	C5	120.0
C4	C5	H7	119.7
C4	C5	C6	120.6(7)
H7	C5	C6	119.7
C5	C6	H1A	120.5
C5	C6	C7	118.9(7)
H1A	C6	C7	120.5
C2	C7	C6	122.0(6)
C2	C7	H5	118.9
C6	C7	H5	119.1
C8	C8	N1	111.5(5)
C8	C8	O3	121.0(6)
N1	C8	O3	127.4(6)
C3	N1	C8	129.8(5)
C3	N1	H1	115.1
C8	N1	H1	115.2

TABLE S-IV. Torsions in compound **(2)**

Atom 1	Atom 2	Atom 3	Atom 4	Torsion, °
O1	C1	C2	C3	177.8(6)
O1	C1	C2	C7	-2.7(9)
O2	C1	C2	C3	-3(1)
O2	C1	C2	C7	176.6(6)
C1	C2	C3	C4	178.9(6)
C1	C2	C3	N1	-1.5(8)
C7	C2	C3	C4	-0.6(8)
C7	C2	C3	N1	179.0(5)
C1	C2	C7	C6	-178.1(6)
C1	C2	C7	H5	2
C3	C2	C7	C6	1.4(9)
C3	C2	C7	H5	-178.3
C2	C3	C4	H6	-179.6
C2	C3	C4	C5	0.5(9)
N1	C3	C4	H6	1
N1	C3	C4	C5	-179.1(6)
C2	C3	N1	C8	-176.5(6)
C2	C3	N1	H1	3.5
C4	C3	N1	C8	3.1(9)
C4	C3	N1	H1	-176.9
C3	C4	C5	H7	178.9
C3	C4	C5	C6	-1(1)
H6	C4	C5	H7	-1
H6	C4	C5	C6	178.9
C4	C5	C6	H1A	-177.9
C4	C5	C6	C7	2(1)
H7	C5	C6	H1A	2
H7	C5	C6	C7	-178.2
C5	C6	C7	C2	-2(1)
C5	C6	C7	H5	177.6
H1A	C6	C7	C2	177.7
H1A	C6	C7	H5	-3
O3	C8	N1	C3	-1(1)
O3	C8	N1	H1	179.2
C8	C8	N1	C3	178.6(5)
C8	C8	N1	H1	-1.4
N1	C8	C8	N1	180.0(5)
N1	C8	C8	O3	0.6(9)
O3	C8	C8	N1	-0.6(9)
O3	C8	C8	O3	-180.0(6)
O1	C1	C2	C3	-177.8(6)
O1	C1	C2	C7	2.7(9)
O2	C1	C2	C3	3(1)
O2	C1	C2	C7	-176.6(6)
C1	C2	C3	C4	-178.9(6)
C1	C2	C3	N1	1.5(8)
C7	C2	C3	C4	0.6(8)

Atom 1	Atom 2	Atom 3	Atom 4	Torsion, °
C7	C2	C3	N1	-179.0(5)
C1	C2	C7	C6	178.1(6)
C1	C2	C7	H5	-2
C3	C2	C7	C6	-1.4(9)
C3	C2	C7	H5	178.3
C2	C3	C4	H6	179.6
C2	C3	C4	C5	-0.5(9)
N1	C3	C4	H6	-1
N1	C3	C4	C5	179.1(6)
C2	C3	N1	C8	176.5(6)
C2	C3	N1	H1	-3.5
C4	C3	N1	C8	-3.1(9)
C4	C3	N1	H1	176.9
C3	C4	C5	H7	-178.9
C3	C4	C5	C6	1(1)
H6	C4	C5	H7	1
H6	C4	C5	C6	-178.9
C4	C5	C6	H1A	177.9
C4	C5	C6	C7	-2(1)
H7	C5	C6	H1A	-2
H7	C5	C6	C7	178.2
C5	C6	C7	C2	2(1)
C5	C6	C7	H5	-177.6
H1A	C6	C7	C2	-177.7
H1A	C6	C7	H5	3
C8	C8	N1	C3	-178.6(5)
C8	C8	N1	H1	1.4
O3	C8	N1	C3	1(1)
O3	C8	N1	H1	-179.2

Coordination sphere of potassium in $K_2H_2obbz \times 2H_2O$ is shown in Fig. S-5.

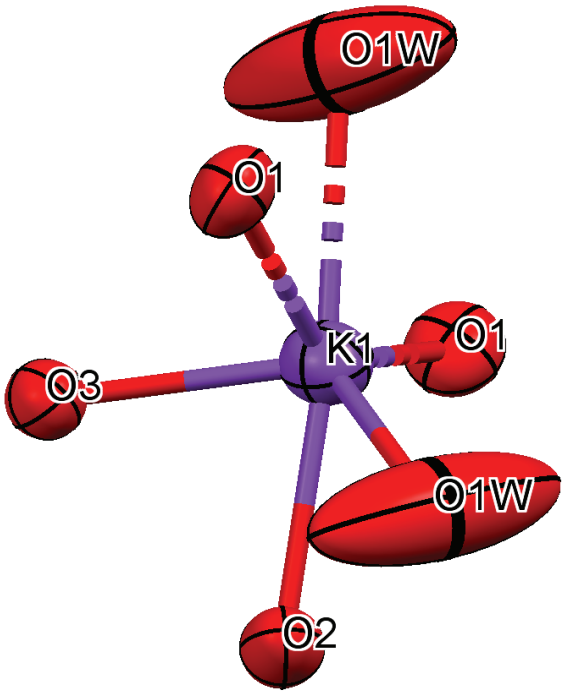

Fig. S-5 Coordination sphere of $K_2H_2obbz \times 2H_2O$.

*2,2'-[(1,2-dioxoethane-1,2-diyl)diimino] dibenzoic acid, H_4obbz (**1**)*[27]

Anal. Calcd. for $C_{16}H_{12}N_2O_6$: C, 58.54; H, 3.68; N, 8.53 %. Found: C, 57.86; H, 3.52; N, 8.49 %. Melting point: 205 °C.

*$K_2H_2obbz{\cdot}2H_2O$ (**2**)*

Anal. Calcd. for $C_{16}H_{10}K_2N_2O_8$: C, 44.03; H, 2.31; N, 6.42 %. Found: C, 43.90; H, 2.28; N, 6.40 %. ^{1}H-NMR (200 MHz, D_2O, δ / ppm): 7.20-7.36 (2H, *m*, ArH), 7.48-7.59 (2H, *m*, ArH), 7.86-7.96 (2H, *m*, ArH), 8.28-8.39 (2H, *m*, ArH). ^{13}C-NMR (50 MHz, D_2O, δ / ppm): 178.8, 150.5, 134.8, 133.8, 127.1, 123.0, 120.6, 120.4. IR (KBr, pellet ν / cm^{-1}): 3268.33m, 1701.35s, 1679.22s, 1581.29s, 1511.12s, 1455.75m, 1406.48s, 1270.68s, 1171.46m, 1147.50m, 1091.24w, 753.54s. Melting point: 217 °C.

REFERENCES

1. *Gaussian 09, Revision A.02,* Gaussian, Inc., Wallingford CT, 2016
2. *Amber 2021*, University of California, San Francisco, CA, 2021
3. A. W. Götz, M. J. Williamson, D. Xu, D. Poole, S. Le Grand, R. C. Walker, *J. Chem. Theory Comput.* **8** (2012) 1542 (https://doi.org/10.1021/ct200909j)
4. R. Salomon-Ferrer, A. W. Götz, D. Poole, S. Le Grand, R. C. Walker, *J. Chem. Theory Comput.* **9** (2013) 3878 (https://doi.org/10.1021/ct400314y)

5. A. D. Becke, *Phys. Rev. A* **38** (1988) 3098 (https://doi.org/10.1103/PhysRevA.38.3098)
6. C. Lee, W. Yang, R. G. Parr, *Phys. Rev. B* **37** (1988) 785 (https://doi.org/10.1103/PhysRevB.37.785)
7. A. D. Becke, *J. Chem. Phys.* **98** (1993) 5648 (https://doi.org/10.1063/1.464913)
8. M. F. Peintinger, D. V. Oliveira, T. Bredow, *J. Comput. Chem.* **34** (2013) 451 (https://doi.org/10.1002/jcc.23153)
9. J. Wang, W. Wang, P. A. Kollman, D. A. Case, *J. Mol. Graph. Model.* **25** (2006) 247 (https://doi.org/10.1016/j.jmgm.2005.12.005)
10. J. Wang, R. M. Wolf, J. W. Caldwell, P. A. Kollman, D. A. Case, *J. Comput. Chem.* **25** (2004) 1157 (https://doi.org/10.1002/jcc.20035)
11. G. M. Morris, R. Huey, W. Lindstrom, M. F. Sanner, R. K. Belew, D. S. Goodsell, A. J. Olson, *J. Comput. Chem.* **30** (2009) 2785 (https://doi.org/10.1002/jcc.21256)
12. A. T. Macias, D. S. Williamson, N. Allen, J. Borgognoni, A. Clay, Z. Daniels, P. Dokurno, M. J. Drysdale, G. L. Francis, C. J. Graham, R. Howes, N. Matassova, J. B. Murray, R. Parsons, T. Shaw, A. E. Surgenor, L. Terry, Y. Wang, M. Wood, A. J. Massey, *J. Med. Chem.* **54** (2011) 4034 (https://doi.org/10.1021/jm101625x)
13. W. L. Jorgensen, J. Chandrasekhar, J. D. Madura, R. W. Impey, M. L. Klein, *J. Chem. Phys.* **79** (1983) 926 (https://doi.org/10.1063/1.445869)
14. P. Li, L. F. Song, K. M. Merz, *J. Chem. Theory Comput.* **11** (2015) 1645 (https://doi.org/10.1021/ct500918t)
15. T. Darden, D. York, L. Pedersen, *J. Chem. Phys.* **98** (1993) 10089 (https://doi.org/10.1063/1.464397)
16. T. E. I. Cheatham, J. L. Miller, T. Fox, T. A. Darden, P. A. Kollman, *J. Am. Chem. Soc.* **117** (1995) 4193 (https://doi.org/10.1021/ja00119a045)
17. H. G. Petersen, *J. Chem. Phys.* **103** (1995) 3668 (https://doi.org/10.1063/1.470043)
18. J.-P. Ryckaert, G. Ciccotti, H. J. . Berendsen, *J. Comput. Phys.* **23** (1977) 327 (https://doi.org/10.1016/0021-9991(77)90098-5)
19. S. Miyamoto, P. A. Kollman, *J. Comput. Chem.* **13** (1992) 952 (https://doi.org/10.1002/jcc.540130805)
20. H. J. C. Berendsen, J. P. M. Postma, W. F. van Gunsteren, A. DiNola, J. R. Haak, *J. Chem. Phys.* **81** (1984) 3684 (https://doi.org/10.1063/1.448118)
21. B. R. Miller, T. D. McGee, J. M. Swails, N. Homeyer, H. Gohlke, A. E. Roitberg, *J. Chem. Theory Comput.* **8** (2012) 3314 (https://doi.org/10.1021/ct300418h)
22. G. D. Hawkins, C. J. Cramer, D. G. Truhlar, *Chem. Phys. Lett.* **246** (1995) 122 (https://doi.org/10.1016/0009-2614(95)01082-K)
23. G. D. Hawkins, C. J. Cramer, D. G. Truhlar, *J. Phys. Chem.* **100** (1996) 19824 (https://doi.org/10.1021/JP961710N)
24. V. Tsui, D. A. Case, *Biopolymers* **56** (2000) 275 (https://doi.org/10.1002/1097-0282(2000)56:4%3C275::aid-bip10024%3E3.0.co;2-e)
25. T. Mosmann, *J. Immunol. Methods* **65** (1983) 55 (https://doi.org/10.1016/0022-1759(83)90303-4)
26. N. Khanna, H. Jayaram, N. Singh, *Life Sci.* **75** (2004) 179 (https://doi.org/10.1016/j.lfs.2003.11.026)
27. M. F. Peintinger, D. V. Oliveira, T. Bredow, *J. Comput. Chem.* **34** (2013) 451 (https://doi.org/10.1002/jcc.23153).